Effect of abrasion and biofouling on aerodynamic performance of industrial surface coatings

F. Gökhan Ergin
Dantec Dynamics, Skovlunde, Denmark, 2740
gokhan.ergin@dantecdynamics.com

ABSTRACT

Effect of abrasion and biofouling on aerodynamics performance of industrial surface coatings is investigated experimentally. The test section of the DTU closed-loop wind tunnel is refurbished to perform automated boundary layer stability experiments. The modifications satisfy the measurement requirements imposed by NATURAL EU project work packages 4 and 5. The design features include a sliding test section front window, a computer-controlled three-axis traverse, angle of attack adjustment, zero-pressure-gradient alignment, quick replacement of test plates and repeatable alignment between plates. Boundary layer profile measurements were performed on pristine, abraded and biofouled flat plates using a constant temperature anemometry system. The anemometers were controlled using state-of-the-art electronics, a computer-controlled hotwire calibrator and LabVIEW. Both laminar and turbulent boundary layer profiles were measured.

INTRODUCTION

The aerodynamic performance of a vehicle is closely linked with its surface roughness. For external surfaces, roughness can lead to increased skin friction drag and reduced lift force. For instance, erosion of aircraft surfaces during routine flight has been claimed to increase fuel consumption and CO2 emissions by almost 5%. Similarly, fouling of ship hulls by marine organisms is estimated to increase fuel consumption by up to 40% [1]. Besides increasing drag, lift can also be compromised leading to similar performance losses. For example for wind turbines operating in cold climates ice accretion can cause a loss of 20-50% of electricity production; whereas for those operating in warmer climates, fouling of the blade leading edge by insects can reduce power production from wind turbines by up to 50% [2]

A variety of surface coatings have been considered to prevent the accumulation of surface roughness. Conventional paints and procedures have not been satisfactory in reducing these effects. New coatings with nanometer-sized powder may be more successful and have significant potential performance improvements. To be successful in the field, any such coating must have good durability. In time under environmental exposure, unwanted changes in the nano-structure often reduces performance via two major mechanisms; fouling and erosion. Surface fouling is caused by external material (e.g. dust/oil, ice, biofouling such as insects, barnacles and algae) building up on the surface, changing the roughness levels, hence reducing performance. Surface erosion (wear and corrosion) is often due to weathering including UV degradation, abrasion and friction cause surface erosion of the coating, leading to loss of material over time, hence a loss of performance associated with loss of active component and change in surface morphology.

Nanomaterial-based paints are interesting as they can both achieve desired roughness levels, and are able to modify the surface energy of the underlying material. Controlling the transition location in boundary layers offers considerable advantages in numerous industrial applications. Using nanomaterial-based coatings, the flow-surface interaction can be engineered to delay the transition of flow to turbulence, and hence reduce flow forces, and save costs for structures such as aerofoils, winglets, wings and wind turbine blades.

The NATURAL project is aimed to develop methods that allow the evaluation of surfaces at the nanoscale and correlate the measured surface structure with aerodynamic performance. The testing technique involves the development of an understanding of the relationship between physical properties of fluid flow at the surface, surface roughness morphology and surface energy (Work packages 4 and 5). This measurement method provides, for the first time, a technique that will allow these novel coatings to be evaluated in a manner that allows nanometer-scale characteristics to be correlated with their effects on the flow behaviour and aerodynamic efficiency.

To achieve the objective of NATURAL Work Packages 4 and 5, the “yellow” wind tunnel in the the Department of Mechanical Engineering at the Technical University of Denmark (DTU) was modified to make boundary-layer profile measurements over a variety of surface samples. Once these modifications were made, 11 different fibreglass samples were fabricated, coated and subjected to typical wear patterns. Six of these plates are tested in pristine condition, (without abrasion or biofouling), two were biofouled in a special environmental chamber, and three were subject to abrasion using sandblasting. One of the pristine plates (FG-P) was not coated. This plate was used achieve the

baseline flow condition: a zero-pressure-gradient (ZPG) laminar boundary layer flow over the entire length. This way the flow field over remaining five pristine nano-coatings can be compared to the baseline flow condition. Similarly, the flow field over abraded and biofouled samples could be compared their pristine counterparts. The overview of samples and a short description is given in Table 1. All plates have dimensions 725mm x 294mm x 10mm and a 25mm-long elliptical leading edge (Fig. 2). Only the FG-P plate has ten Ø3mm pressure taps for ZPG alignment.

Table 1. Overview of the pristine (P), abraded (A) and biofouled (B) samples.

Sample	Description
FG-P	Fiber Glass – Pristine
K-P	Coating 1 – Pristine
2-P	Coating 2 – Pristine
2I-P	Coating 2 + I nanoparticles – Pristine
2O-P	Coating 2 + O nanoparticles – Pristine
2R-P	Coating 2 + R nanoparticles – Pristine
2-B	Coating 2 + Biofouled
2I-B	Coating 2 + I nanoparticles – Biofouled
2-A	Coating 2 – Abraded
2O-A	Coating 2 + O nanoparticles – Abraded
2R-A	Coating 2 + R nanoparticles – Abraded

TEST SECTION DESIGN

The wind tunnel facility used during the experiments is the "yellow" wind tunnel belonging to the Department of Mechanical Engineering at the Technical University of Denmark (DTU). The facility is a closed-loop subsonic facility erected in 1976, with a nominal maximum flow speed of 60 m/s and a measured background turbulence intensity level of 0.15% at 20m/s. The contraction ratio is 12.94:1, the nominal test section dimensions are 0.3 m × 0.3 m × 0.75m, with an increasing cross sectional area along the streamwise direction to compensate for developing boundary layers. Although the wind tunnel is equipped with a cooling system for the drive fan, the temperature of the flow cannot be controlled during the experiments. As a result, the air temperature in the tunnel rises from approximately 22°C to 26°C during the course of the experiments. Two interchangeable test sections are available which enables a quick change to a different experimental setup. One of these test sections was modified to meet the boundary layer measurement requirements imposed by the NATURAL EU project work packages 4 and 5. These requirements include (i) automated measurement of laminar, transitional and turbulent boundary layer profiles, (ii) angle of attack adjustment from outside the test section, (iii) zero-pressure-gradient alignment during tunnel operation, (iv) quick replacement of test plates and (v) maintaining alignment between plates, (vi) minimum flow disturbance and vibrations due to probe support equipment (vii) real-time normalisation of boundary layer velocity using the freestream velocity.

Automated positioning

According to Ref. [3] and Ref. [4], as of 2008 there are 14 out of 383 wind tunnels that are equipped with an automated sensor positioning system. With the automated positioning system described here, the DTU Yellow wind tunnel is the 15th known (other wind tunnels may have been equipped with such a system since 2008) wind tunnel with this capability.

The automated positioning of sensors was achieved using a custom-built three-axis traversing mechanism. The final design is shown in Fig. 1a and the actual mechanism mounted on the DTU wind tunnel is shown in Fig. 1b. The shorter y-axis lead screw is attached on the longer x-axis lead screw in the horizontal plane. The x-axis lead screw is attached on two vertical lead screws of the z-axis traverse mechanism. The z-axis lead screws are driven by a single stepper motor and the power distribution is achieved by the drive shaft connecting two gearboxes, the cyan colored parts in Fig. 1a. The minimum step size in each direction is 6.25µm with a positioning accuracy of 1µm. The hotwire support arm is attached on the y-axis of the traverse accessing the test section through a streamwise slit cut in the front window. The streamwise slit on the sliding front window is sealed with during each measurement in order to avoid flow through the slit (Fig. 1b).

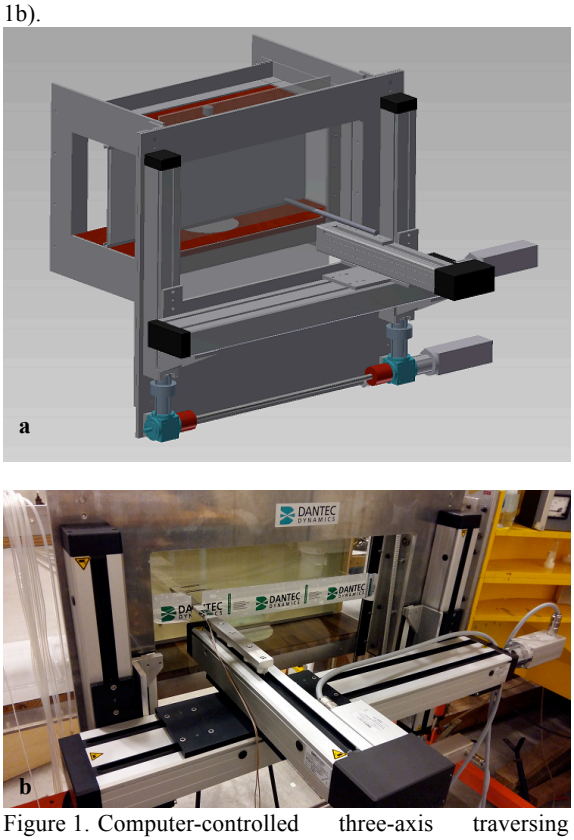

Figure 1. Computer-controlled three-axis traversing system (a) the design schematic (b) the actual unit.

Sealing the slit during experiments implies that measurements can be taken in cross-sectional y-z planes perpendicular to the flow direction. The flat plate schematic, assumed coordinate system and the measurement planes are shown in Fig. 2. Traverse movements in the y-direction is simply through the

opening between duct tape and through the streamwise slit. However, in order to achieve traversing movements in the z-direction requires a sliding front window coupled with the z-axis lead screws. The sliding front window is placed in a vertical rail on the test section and is pulled up and down using a pulleys and belts (Fig. 1b) The negative pressure inside the test section helps seal the window on the test section frame.

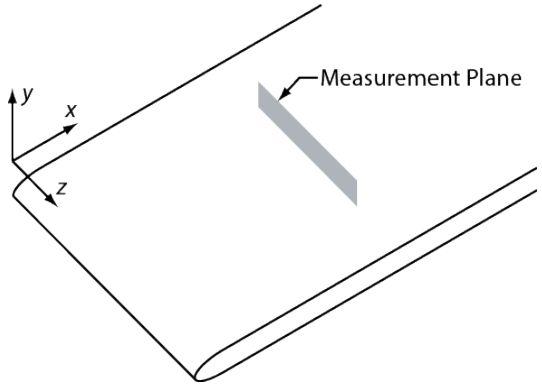

Figure 2. Flat plate schematic, assumed coordinate system and the measurement plane.

Angle of attack adjustment

The flat plates with elliptical leading edges are mounted vertically in the test section in order to minimize dust collection over time (Fig. 3a). Using special removable fixtures and guide rails, the plates are mounted on two freely rotating carousels, one on the bottom, and one on the top wall of the test section. The angular orientation of the plate with respect to the incoming flow can be changed by rotating a micrometer screw on the top of the test section (Fig. 3b). The angle indicator provides a course scale and the micrometer provides a finer scale for precise angle of attack adjustments. Zero angle of attack was used during the experiments performed in this work.

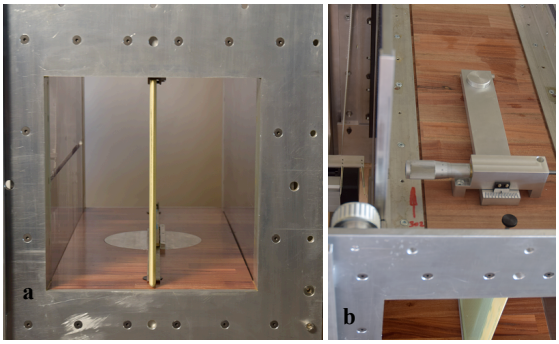

Figure 3. (a) Test section view as seen by the flow, (b) angle of attack adjustment for the plate carousel and the angle indicator.

Zero pressure gradient alignment

One of the pristine flat plates (FG-P) is used for the zero pressure gradient (ZPG) alignment. This plate was not coated and therefore has a smooth flat surface finish that can produce a laminar boundary layer profile over the entire length for a tunnel speed of 20m/s. The alignment plate is tapped with 10 holes for pressure readings, 5 closer the bottom and 5 closer to the top of the plate (Fig. 4a). Pressure readings along the plate are taken in order to satisfy the ZPG requirement (Fig. 4b).

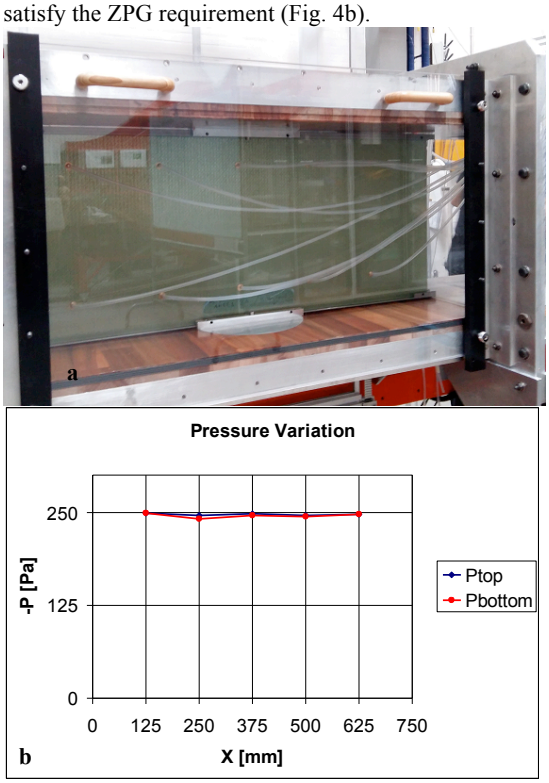

Figure 4. (a) Back of the alignment plate during ZPG alignment, (b) pressure variation along the plate.

Quick plate replacement and repeatable alignment

It is essential to install a new test plates in a reasonable amount of time and without changing the alignment. For repeatable alignment, the plates are mounted on two guide rails using a total of seven setscrews, fixed on the bottom and top carousels (visible in Fig. 3a and 4a). Once the ZPG alignment is performed, the guide rail positions are locked using four setscrews, one at each corner of the plate. One of these setscrews (front top corner) is visible in Fig. 3b. For quick replacement, the plates are mounted on the rails using special removable fixtures (visible in Fig. 3a).

Minimizing flow disturbance and flow induced vibrations

The hotwire support arm profile is streamlined to minimize the flow disturbances (Fig 5a). The leading edge is machined in a bluff semi circular shape and the trailing edge is tapered to resemble an aerofoil shape. The hotwire cables were placed in a groove cut along the trailing edge. The probes could be inserted / replaced by retracting the hotwire support arm fully out through the slit, i.e. without having to remove the plate in the test section (Fig 5a). In order to minimize flow induced vibrations the hotwire probe support lengths were kept short (Fig 5b). The boundary layer probe support has a 5deg angle with respect to the flow direction in order to keep safety a

margin between the flat surface and the tip of the support arm.

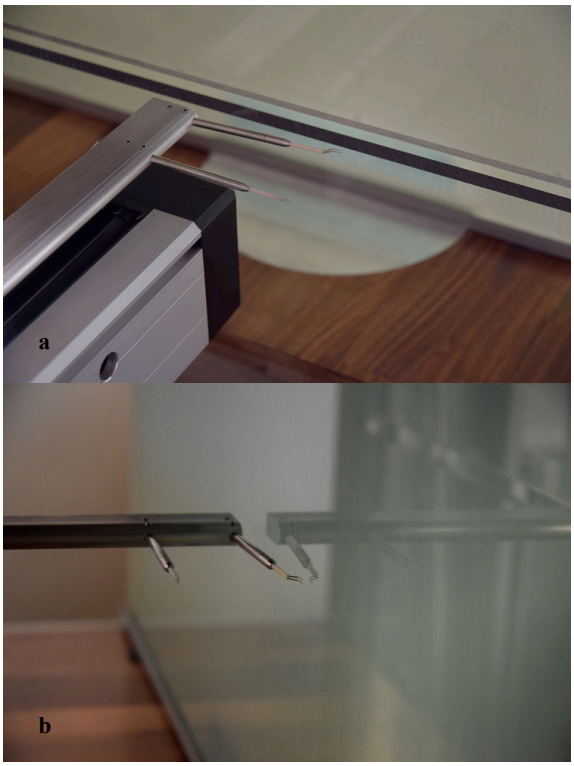

Figure 5. Boundary layer and freestream hotwire probes (a) during insertion into probe support outside the test section, (b) during measurements in the boundary layer.

MEASUREMENT SYSTEM

The measurement system is a constant-temperature anemometer (CTA) system manufactured by Dantec Dynamics (DD, Skovlunde Denmark). The system consists of a StreamLine Pro Frame and Controller with three CTA velocity channels, StreamLine Pro Automatic Calibrator with Nozzle I, a Pitch/Yaw – Roll (PYR) manipulator to perform velocity calibrations, StreamWare Pro software and a custom-developed LabVIEW program. The system controller is a Dell Optiplex 990 PC with an Intel Core i7-2600, 3.4GHz CPU and 8GB Ram, running on a 64-bit Windows 7 Enterprise SP1 operating system. The measured voltages were transferred to the computer via a National Instruments 4-channel simultaneous sampling differential USB A/D converter. The 55P15 boundary layer probe and the 55P11 freestream probe are positioned at multiple grid points using a computer-controlled 3-axis traversing system. Both probes are mounted on the traversing mechanism using the hotwire support arm.

The 1:20 bridge configuration is selected for high sensitivity on the CTA electronics. The probe was placed in the vertical free jet with a flat, low-turbulent velocity profile during the velocity calibration. Nozzle I was used to cover a velocity range of 1-60m/s. StreamWare Pro was used for the velocity calibration process, and Labview programs were used for measuring laminar and turbulent velocity profiles. The linearization of voltages was performed using a 5th order polynomial. Since the temperature in the test section may rise as much as 5°C during the course of the measurements, temperature correction was performed using a correction procedure suggested by Benjamin and Roberts [5]. Voltages were corrected according to

$$V_c = V_m \left[1 - \frac{T_c - T_x}{T_w - T_x} \right]^{0.55} \quad (1)$$

where V_c is the corrected voltage, V_m is the measured voltage, T_c is the calibration temperature, T_w is the wire temperature and T_x is the elevated ambient temperature during measurements.

Experiments were conducted on 4 measurement planes for each plate; 125mm, 250mm, 375mm and 500mm from the plate leading edge. Boundary layer velocity was normalised with the freestream velocity in order to minimize the effect of freestream speed fluctuations. The boundary layer type was identified for each plane before the actual experiment by measuring a boundary layer profile on each edge and in the middle. The measurement height was set to either η=8 (laminar) and η=16 (turbulent) depending on the boundary layer type. Corrections of arbitrary wall normal coordinates were performed according to Ref. [6]. Wall position at each spanwise location is estimated by fitting a line to the velocity profile between data points where the velocity is 30% of the freestream velocity, U_{fs}, to 18% of that value then extrapolating to zero velocity. Then a quadratic fit is performed on the wall positions vs. spanwise coordinate and this information is used for correcting the wall-normal positions of the acquired data. The difference between Ref. [6] and the current study is the number of points used in the quadratic fit. In Ref. [6], because of the presence of the roughness array, the wall location estimates were made at three spanwise positions between neighbouring roughness elements, and at two spanwise positions at each end of the spanwise range (Fig. 2 in Ref [6]). Here, due to the presence of distributed roughness, all spanwise positions were used for the quadratic fit. This is useful in two aspects: first the number of data points is increased for a better wall location estimate, and second this approach provides an unambiguous definition of an effective wall surface in the presence of distributed roughness. Finally the data files are saved in .txt format compatible with Tecplot. As an example, a data file header and first few lines of data is included in Appendix A1. The overview of measurement range and resolution for the experiments are provided in Table 2.

Table 2. Measurement range and resolution

Sample	Spanwise range, z and resolution [mm]	Wall-normal range η and resolution
FG-P	–25 to +25, 1mm	0 to 8, 0.1
K-P	–25 to +25, 1mm	0 to 8, 0.1
2-P	–25 to +25, 1mm	0 to 8, 0.1
2I-P	–25 to +50, 5mm	0 to 16, 0.1
2O-P	–25 to +25, 1mm	0 to 8, 0.1
2R-P	–25 to +25, 1mm	0 to 8, 0.1
2-B	–50 to +50, 2.5mm	0 to 8, 0.1
2I-B	–50 to +50, 2.5mm	0 to 16, 0.1
2-A	–50 to +50, 2.5mm	0 to 16, 0.1

2O-A	–50 to +50, 2.5mm	0 to 16, 0.1
2R-A	–50 to +50, 2.5mm	0 to 16, 0.1

RESULTS

The results are presented as time-averaged steady flow field and the unsteady fluctuations. The steady flow field is represented by iso-velocity lines, with 10% increments of the normalized boundary layer velocity; i.e. 0.1Ufs, 0.2Ufs, 0.3Ufs, 0.1Ufs … 0.9Ufs. The unsteady flow field is represented by colored contour maps with the corresponding contour palette in each (sub)figure.

The following comparisons are made:

1. Comparison of flow field among 6 Pristine plates
2. Comparison of flow field among 3 Abraded plates
3. Comparison of flow field between two Biofouled plates
4. Comparison of flow field on 2I coating in Pristine and Biofouled state
5. Comparison of flow field on 2O coating in Pristine and Abraded state
6. Comparison of flow field on 2R coating in Pristine and Abraded state
7. Comparison of flow field on Plate 2 in Pristine, Abraded and Biofouled state

First, a comparison among 6 pristine plates is made in order to assess the performance in pristine state: All pristine plates except 2I produced a laminar boundary layer with minimal turbulence intensity throughout the domain. Only the 2I plate produced a turbulent boundary layer in one partition of the measurement region (Fig. 7). The streamwise spreading of the turbulent spot is also clear: The turbulent spot appears on the right edge of the measurement domain at x=250mm, then spreads leftwards covering approximately half of the z-domain at x=375mm, and covering approximately three quarters of the z-domain at x=500mm. This indicates that the 2I plate has sufficiently large localized roughness levels already in the pristine state to trigger turbulent flow in the boundary layer. The spread angle for this turbulent spot is calculated as ~9° with respect to the x-axis in the x-z plane.

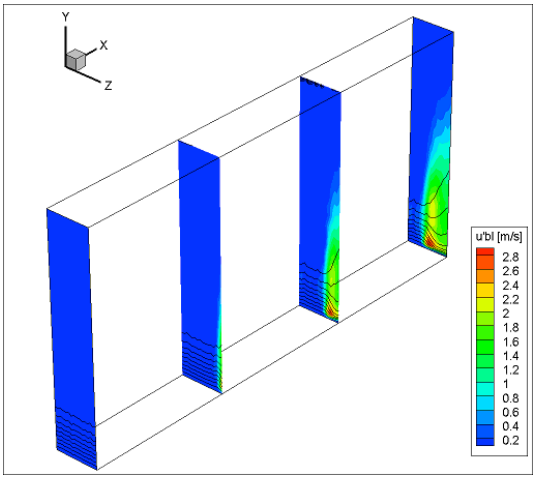

Figure 7. Flow field over the pristine 2I plate.

Second, a comparison among the 3 abraded plates is made in order to assess the performance in the abraded state: Interestingly, all abraded plates produced laminar boundary layer profiles. The abrasion via sandblasting certainly increased the roughness level for smoother pristine plates, but not enough to reach the critical roughness levels to trigger turbulence. The sandblasted surfaces were found to have a homogenous and subcritical roughness levels. This raises an interesting question: "Can abrasion via sandblasting also reduce roughness levels of supercritically rough surfaces in their pristine condition (such as the 2I plate). Unfortunately the 2I plate was not tested in the abraded state, and this question will be the focus of future examinations.

Third, a comparison between each biofouled plate is made to assess the performance after aging. The biofouled plate 2 produced a laminar flow whereas the biofouled 2I plate produced a turbulent flow in most of the domain (Fig. 8). The spreading angle for this turbulent spot is calculated as ~8° w.r.t. the x-axis in the x-z plane.

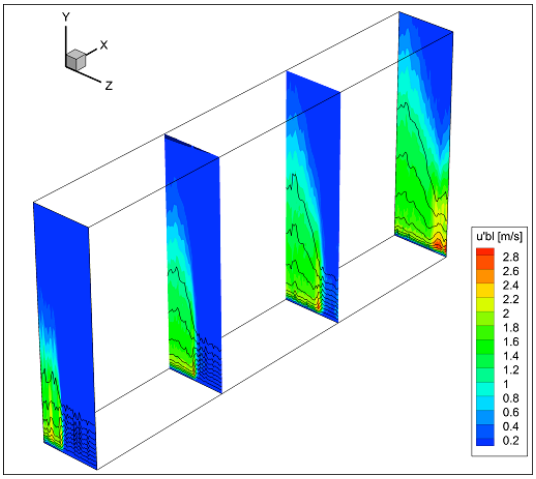

Figure 8. Flow field measured on biofouled 2I plate

Since the 2I-coated plate produces turbulence in the boundary layer both in its pristine state and in the biofouled state, a comparison of flow fields can reveal qualitative effects of biofouling (Fig. 9, left: pristine, right: biofouled). Upon comparison of the flow fields, the first observation is that the turbulence is observed already at x=125mm, and the flow fluctuations cover half of the measurement domain. This means the turbulent spots for the biofouled plate appear much closer to the leading edge, and this could be because of the combined effect of supercritical roughness levels due to the coating and biofouling. The similarity in the spreading angles (~8° and ~9°) is also visible in Fig. 9.

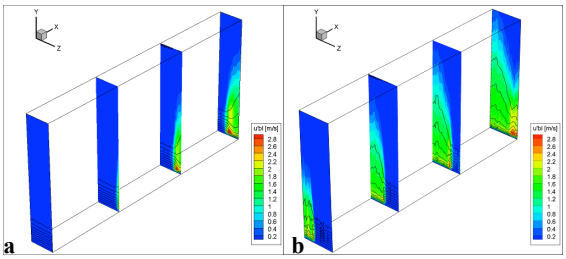

Figure 9. Comparison of flow field over 2I coating in Pristine (left) and Biofouled (right) state

The 2O and 2R coatings were tested in their pristine and abraded states. In both tests, both plates produced laminar boundary layer profiles regardless of their condition. These two coatings equally provide very good overall performances in terms of flow disturbances in the boundary layer. These two plates were not tested in the biofouled state.

Finally the plate with coating 2 was tested in all three states; i.e. in pristine, abraded and biofouled states. Plate 2 produced laminar boundary layer profiles in all states and therefore coating 2 provides the best overall performance, by producing the least amount of flow disturbances in the boundary layer.

CONCLUSIONS AND FUTURE WORK

Since the objective of the NATURAL project is to identify coating(s) which can keep their initial surface structure in their aged (biofouled and/or abraded) state, a performance criterion can be defined by its aerodynamic performance: If the coating can produce a laminar boundary layer in its pristine state and can keep this type of flow in its aged state, the coating is successful. In contrast, if a coating cannot produce a laminar boundary layer profile in its pristine condition or keep it in its aged condition, then the coating is not successful. Based on this argument, three main conclusions can be reached:

- Coating 2 (which does not contain nanoparticles) is the most successful since it is able to produce a laminar boundary layer and keep this flow condition in its aged state (both biofouled and abraded).
- Coating 2O and 2R are successful since they are able to produce a laminar boundary layer and keep this flow condition in their abraded state. Since these panels were not biofouled no definitive conclusion can be made on their success in the biofouled state.
- Coating 2I is unsuccessful as it produces a turbulent boundary layer in its pristine and aged state. Since this panel was not abraded no definitive conclusion can be made on its success in the abraded state.

Future investigations will be focused on three subjects (i) measurement of multiple velocity components in the boundary layer and (ii) how the distributed surface roughness of an individual coating is linked to the flow field it produces. (iii) Although panel 2I was not abraded, since it produces a turbulent boundary layer already in its pristine stage due to high roughness amplitudes, there is a chance that that the abrasion could have produced a better result (such as a delayed transition location, at least) by reducing the surface roughness amplitude.

ACKNOWLEDGMENTS

The research leading to these results has received funding from the European Union Seventh Framework Program (FP7 2007-2013) under grant agreement number 310397. The author thanks Allan Kruse Christensen for making the engineering drawings and for his efforts during manufacturing and installation, and Prof. Edward B. White for reviewing the manuscript and Prof. Knud Erik Meyer for providing access to the wind tunnel.

REFERENCES

[1] D. Kane “Hull and Propeller Performance Monitoring: Fuel Conversion and Emissions Reduction”, in Climate Change and Ships: Increasing Energy Efficiency, Proceedings, SNAME, February 16-17, 2010.

[2] N. Dalili, A. Edrisy, R. Carriveau. “A review of surface engineering issues critical to wind turbine performance” Renewable and Sustainable Energy Reviews 13 (2009) 428–438

[3] M. Goodrich, J. Gorham, N. Ivey, S. Kim, M. Lewis, C. Minkus. “Wind Tunnels of the Eastern Hemisphere” A Report Prepared by the Federal Research Division, Library of Congress for the Aeronautics Research Mission Directorate, National Aeronautics and Space Administration, August 2008

[4] M. Goodrich, J. Gorham. “Wind Tunnels of the Western Hemisphere” A Report Prepared by the Federal Research Division, Library of Congress for the Aeronautics Research Mission Directorate, National Aeronautics and Space Administration, June 2008

[5] SF Benjamin, CA Roberts “Measuring flow velocity at elevated temperature with a hot wire anemometer calibrated in cold flow” Int. Journ. of Heat & Mass Transfer 45 (2002) 703 – 706

[6] EB White, FG Ergin “Using laminar-flow velocity profiles to locate the wall behind roughness elements” Experiments in Fluids 36 (2004) 805–812

APPENDIX A1. A SAMPLE DATA FILE

TITLE = "FG-P"
VARIABLES = "eta" "z [mm]" "x [mm]" "Ubl/Ufs" "u'bl [m/s]"
ZONE T="Natural Data" I=81 J=51 K=4 f=point

0	-25	125	0	0
0.1	-25	125	0.0382	0.0093
0.2	-25	125	0.0764	0.0186
0.3	-25	125	0.1146	0.0278
0.4	-25	125	0.1528	0.0371
0.5	-25	125	0.1896	0.0376
0.6	-25	125	0.2252	0.0437
0.7	-25	125	0.2621	0.0554
0.8	-25	125	0.299	0.056
0.9	-25	125	0.3356	0.062
1	-25	125	0.3734	0.0736

…